Multivariate ratio analysis and DNA markers reveal a new Australian species and three synonymies in eucalypt-gall-associated *Megastigmus* (Hymenoptera: Megastigmidae)

Ngoc Hoan Le[1] (iD), Helen F. Nahrung[1] (iD), Jess A. T. Morgan[2] and Simon A. Lawson[1] (iD)

[1]Forest Industries Research Centre, University of the Sunshine Coast, Sippy Downs, QLD 4556, Australia and [2]Department of Agriculture and Fisheries, EcoSciences Precinct, PO Box 267, Brisbane Queensland 4001, Australia

Abstract

The genus *Megastigmus* Dalman, 1820 (Hymenoptera: Megastigmidae) contains potential biocontrol agents of the invasive eucalypt galling chalcid *Leptocybe* spp. (Hymenoptera: Eulophidae), with several species reported in various parts of the world. Species discrimination is challenging due to intraspecific morphological variation, difficulty in measuring sizes of body parts, and the lack of information regarding the global distribution of parasitic *Megastigmus*. We used two species commonly associated with *Leptocybe* in its native range to review taxonomic methods and determine the most reliable morphological characters in species delimitation. We examined size variation of body characters, and conducted species discrimination using multivariate ratio analysis, mitochondrial Cytochrome c oxidase subunit 1 (COI) and nuclear 28S rDNA (28S) sequences. Morphological traits were effective in species delimitation yet revealed high variation in several characters employed in current keys. Knowledge generated on morphology and DNA justified the description of a new species, *M. manonae,* sp. n., the first record of *M. pretorianensis* in Australia, and revised diagnostic characters for *M. zvimendeli*. Based on these diagnostic characters and molecular data, we synonymize three species (*M. judikingae,* syn. n., from Australia, *M. sichuanensis,* syn. n., from China and *M. icipeensis,* syn. n., from Kenya) with *M. zvimendeli*. Our findings highlight the importance of molecular markers in assisting taxonomic decision-making and the need for coordinated work in identifying *Megastigmus* associated with *Leptocybe* spp.

Introduction

The invasive eucalypt galling insect *Leptocybe invasa* (Hymenoptera: Eulophidae) was described in 2004 and subsequently identified as two cryptic lineages: a Western lineage (lineage A) and a Chinese lineage (lineage B) (Nugnes *et al.*, 2015; Dittrich-Schröder *et al.*, 2018). These wasps induce swellings in midribs and leaf petioles of young eucalypts causing abnormal growth, and in severe cases, death in seedlings of several economically important species (Mendel *et al.*, 2004; FAO, 2012; Branco *et al.*, 2016). Some Australian parasitic eulophid wasps (Hymenoptera: Eulophidae), *Selitrichodes kryceri, Quadrastichus mendeli* (Kim *et al.*, 2008) and *S. neseri* (Kelly *et al.*, 2012), are used as *Leptocybe* spp. biocontrol agents. These have been reared, released, monitored and, to different extents, reported to occur adventively in numerous countries (Mendel *et al.*, 2017; Huang *et al.*, 2018; Le *et al.*, 2018).

The genus *Megastigmus* (Hymenoptera: Megastigmidae) (Janšta *et al.*, 2018) also contains potential biocontrol agents of *Leptocybe* spp. (Protasov *et al.*, 2008; Doğanlar and Hassan, 2010; Le *et al.*, 2018). Currently, 145 valid *Megastigmus* species are described, of which about one-third are recorded only in Australia, and four shared between Australia and other countries (Noyes, 2020). Nineteen *Megastigmus* species are reported as *Leptocybe* associates: seven endemic Australian species and twelve non-Australian 'local' species thought to represent host-switches in *Leptocybe*'s invasive range (Huang *et al.*, 2018; Le *et al.*, 2018). Two Australian species, *M. zvimendeli* and *M. lawsoni*, were released in Israel where they contribute to the control of *L. invasa* populations (Mendel *et al.*, 2017). Among the non-Australian species, *M. leptocybus* was identified as a potential *L. invasa* biocontrol agent in the Mediterranean (Viggiani *et al.*, 2002; Mendel *et al.*, 2004; Le *et al.*, 2018), while *M. dharwadicus* in India and *M. thitipornae* in Thailand were described and trialled for *Leptocybe* spp. biocontrol (Narendran *et al.*, 2010; Ramanagouda *et al.*, 2011; Sangtongpraow and Charernsom, 2013). *Megastigmus zebrinus*, of Australian origin (Grissell, 2006), is thought to associate with *Leptocybe* in all infested continents except Europe (Grissell, 2006; Doğanlar, 2015; Hernández *et al.*, 2015).

In the pre-*Leptocybe* period, almost all entomophagous *Megastigmus* records were Australian, with only three of twenty-four entomophagous species found outside Australia, none of which associated with Hymenoptera or eucalypts (Grissell, 1999). In contrast, non-Australian *Megastigmus* were mainly phytophagous (Milliron, 1949; Grissell, 1999; Roques and Skrzypczyńska, 2003). The recent associations of local *Megastigmus* with invasive *Leptocybe* thus suggests the occurrence of a previously unknown non-Australian entomophagous group. Considering the Australian origin of eucalypts and *Leptocybe* spp., this could be attributed to rapid host-shift of previously undescribed *Megastigmus* species outside Australia, and/or invasion of undescribed Australian *Megastigmus* species with or following the introduction of host *Leptocybe*. Understanding the drivers behind these novels *Megastigmus-Leptocybe* association is important and requires species confirmation as a prerequisite.

Progress in identifying *Megastigmus* species was made by Doğanlar (Doğanlar and Hassan, 2010; Doğanlar, 2015), who described and redescribed eucalypt-associated *Megastigmus* species in Australia and in many parts of the world, including *M. zvimendeli* as the most extensively used *Megastigmus* species in biocontrol programs worldwide (Mendel *et al.*, 2017; Le *et al.*, 2018). Although taxonomical keys are available, significant challenges remain in species identification. Separation at several dichotomous couplets relies mainly on the size and ratio of body parts, however, variation in sizes and shapes of parasitoid *Megastigmus* is not well understood, resulting in taxonomical uncertainty. Additionally, molecular markers have not been used despite their increasing importance in taxonomy (DeSalle *et al.*, 2005; Hajibabaei *et al.*, 2007) and in *Megastigmus* studies (Auger-Rozenberg *et al.*, 2006; Roques *et al.*, 2016).

To address these challenges, we analyse morphology and species delimitation of Australian parasitic *Megastigmus* using *M. zvimendeli* as a case study, against its sibling *M. manonae*, sp. nov., described herein. Specimens of these two species are measured and analysed using multivariate ratio analysis (MRA) (Baur and Leuenberger, 2011) and DNA-based species delimitation. Our study provides robust insights into *Megastigmus* morphology, which plays a major role in resolving their identities for biocontrol studies.

Materials and methods

Materials

Specimens were collected in roadside surveys between February 2015 and January 2019 in eastern Australia. Gall-bearing young shoots and leaves of eucalypts were collected and assigned codes linked to a database recording collection date, coordinates, gall type and plant details. Galls were placed in zip-lock bags, stored in a cooled insulated box and transferred to the laboratory within 7 days of collection. In the laboratory, galls were placed in separate plastic emergence vials containing moistened tissue paper. Vials were kept in a controlled temperature cabinet maintained at 25 ± 2°C, 50–70% RH for approximately 30 days until no further insect emergence was recorded. Emerging *Megastigmus* wasps were placed in small glass vials containing 100% ethanol (volumetric ratio of insect: ethanol <1:10) and stored at −20°C.

Specimens of the target species (*Megastigmus zvimendeli* and a commonly collected, previously undescribed sibling, described herein as *M. manonae* sp. nov.) were used for morphometric and DNA analyses. All collected females were used in analyses, except those that were physically damaged, and with the exception of collection sites at Miva, QLD and Nanango, QLD, for which 41 and 25 specimens were analysed, respectively. Specimens from each locality used in morphometric analyses and representative specimens from morphometric measurement were subsequently used for molecular analyses. Additional DNA extractions were performed on non-Australian specimens supplied by colleagues in South Africa, China, Israel and Kenya; and Australian specimens from locations where specimen scarcity precluded morphometric examination.

Details of specimens extracted for DNA are provided in Supplementary Document 1.

Morphometric measurement

Measurements were taken for 39 body characters, detailed in table 1 and fig. 1. Terminology follows Baur *et al.* (2014), Bouček (1988), Gibson *et al.* (1998), Graham (1969), and Roques and Skrzypczyńska (2003). In total, 97 specimens (58 *M. zvimendeli*, 39 *M. manonae*) were examined.

Microscopic observations and photographs were taken under a binocular microscope (NIKON SMZ800N) with an attached digital camera (TUCSEN H500), resolution 2584 × 1936 pixels. For measurement, body parts were placed so that the entire length was oriented on an imaginary plane perpendicular to the viewing (photographing) angle. Sizes were measured in pixels by the software Image-Pro® (Media Cybernetics) and ImageJ 1.52a (National Institute of Health, USA) and converted to mm using an object micrometre (Carl Zeiss 5 + 100/100 mm) for species description. If curved, ovipositor and antenna lengths comprised the total length of straight segments approximating the curvature of these parts.

One commonly used trait, *scape length*, was not measured due to difficulties in taking measurable photos without breaking apart the insect body. Similarly, *ppd.l* and *pnc.l* were removed from analysis due to failure in taking reliable measurements.

Measurement data are provided in Supplementary Document 2.

Multivariate ratio analysis

Body ratios were examined by the tool MRA, which analyses body proportions of morphologically similar arthropod species (Baur and Leuenberger, 2011). Body ratios with best discriminant power were determined using the algorithm linear discriminant analysis (*LDA*) *ratio extractor*. Structure of variation of all specimens was analysed by the algorithm *PCA in shape space*, identifying the principal components accounting for variation in shape space, and principal component analysis (*PCA*) *ratio spectrum* which visualizes the contribution of each character (Baur and Leuenberger, 2011). Computation was conducted in R statistical software R studio version 1.2.5019 (RStudioTeam, 2019). Codes for analysis were obtained from Baur and Leuenberger (2011) and the package MASS (Ripley *et al.*, 2018).

DNA extraction, polymerase chain reaction (PCR) and sequencing

DNA was extracted from entire insects using ISOLATE II Genomic DNA Kit (Bioline, Eveleigh NSW, AUS), or a prepGEM® Insect kit (ZyGEM, Hamilton, Aotearoa, NZ), eluting into 40 µl extraction volume. Undiluted genomic DNA was used in PCR amplification using MyTaq™ HS Red DNA Polymerase

Table 1. Body characters of female *Megastigmus* measured for multivariate ratio analysis

| Abbreviation	Terminology	Description	Terminology reference
ool.l	Length of ocellocular line	Shortest distance between a posterior ocellus and eye margin, dorsal view	Graham (1969), Baur *et al.* (2014)
lol.l	Length of lateral ocellar line	Shortest distance between the anterior and a posterior ocellus, dorsal view (also MOL)	Gibson *et al.* (1998)
pol.l	Length of posterior ocellar line	Shortest distance between two posterior ocelli, dorsal view	Graham (1969), Baur *et al.* (2014)
hea.hl	Head height lateral view	Dorsal-ventral distance from where the malar sulcus enters mouth margin to the level of posterior ocelli, lateral view (fig. 1i)	
eye.h	Eye height	Greatest length of eye height, lateral view (fig. 1i)	Baur *et al.* (2014)
eye.b	Eye breadth	Greatest breadth of eye, lateral view (fig. 1i)	Baur *et al.* (2014)
eye.d	Eye distance	Shortest distance between eyes, dorsal view (fig. 1b)	Baur *et al.* (2014)
head.b	Head breadth	Breadth of head from dorsal view, measured at posterior margin of eyes. (fig. 1b)	Baur *et al.* (2014) (modified)
stg.l	Length of stigma knob	The greatest distance between the anterior and posterior edges of the stigma knob, i.e. length of an imaginary line connecting two well-defined edges of the stigma knob running perpendicular/sub-perpendicular to the parastigmal vein (fig. 1c)	Bouček (1988) (terminology for stigma knob, p. 28)
stg.b	Breadth of stigma knob	The greatest distance between two edges of the stigma knob at the basal-apical direction, parallel/sub-parallel to parastigmal vein (fig. 1c)	Bouček (1988) (terminology for stigma knob, pp. 28)
pdl.flg	Pedicel + flagellum	Combined length of pedicel plus flagellum, outer aspect (fig. 1e)	Graham (1969), Baur *et al.* (2014)
fun.l	Length of funicle segment *n*th	Greatest distance between the basal and apical edges of funicle segment number *n* (*n* = 1 to 7) (fig. 1f)	Roques and Skrzypczyńska (2003)
fun.b	Breadth of funicle segment *n*th	Greatest distance between two lateral edges of funicle segment number *n* (*n* = 1 to 7), forming an imaginary line perpendicular to the basal-apical axis of the funicle segment (fig. 1f)	Roques and Skrzypczyńska (2003)
clv.l	Clava length	Shortest distance from the apical tip to the basal edge of clava (fig. 1f)	Gibson *et al.* (1998)
clv.b	Clava breadth	Greatest distance from two lateral edges of clava (fig. 1f)	Gibson *et al.* (1998)
ped.l	Pedicel length	Distance from the basal edge to the apical edge of pedicel (fig. 1f)	Gibson *et al.* (1998)
ped.b	Pedicel breadth	Greatest distance between two lateral edges of pedicel, forming an imaginary line perpendicular to the basal-apical axis of pedicel (fig. 1f)	Gibson *et al.* (1998)
pnc.b	Pronotal collar breadth	Distance between two lateral edges of pronotal collar, dorsal view (fig. 1d)	Graham (1969)
pnc.l	Pronotal collar length (excluded from analysis)	Distance between the anterior and posterior edges of the pronotal collar (fig. 1d)	Graham (1969)
msc.l	Length of mesoscutum	Length of mesoscutum along median line from anterior edge to posterior edge of mesoscutum, dorsal view (fig. 1d)	Baur *et al.* (2014) (modified)
msc.b	Mesoscutum breadth	Greatest breadth of mesoscutum just in front of level of tegula, dorsal view (fig. 1d)	Baur *et al.* (2014)
mss.ll	Length of mesosoma from lateral view	Length of mesosoma along median line from the junction between neck and occiput to the posterior edge of nucha, lateral view (fig. 1a)	Baur *et al.* (2014) (modified)
sct.l	Scutellum length	Length of scutellum along median line from posterior edge of mesoscutum to posterior edge of scutellum, dorsal view (fig. 1j)	Baur *et al.* (2014)
sct.b	Scutellum breadth	Greatest breadth of scutellum, dorsal view (fig. 1j)	Graham (1969)
ppd.l	Propodeum length (excluded from analysis)	Length of propodeum measured along median line from anterior edge to posterior edge of nucha, dorsal view (fig. 1j)	Graham (1969)
gst.ll	Gaster length from lateral view	Length of gaster from anterior edge of the third abdominal segment (the segment posterior to petiole) to the start of the exerted part of ovipositor, from lateral view (fig. 1g)	Baur *et al.* (2014) (modified)
ovi.l	Ovipositor length	Length of the exerted part of ovipositor (fig. 1h)	Roques and Skrzypczyńska (2003)
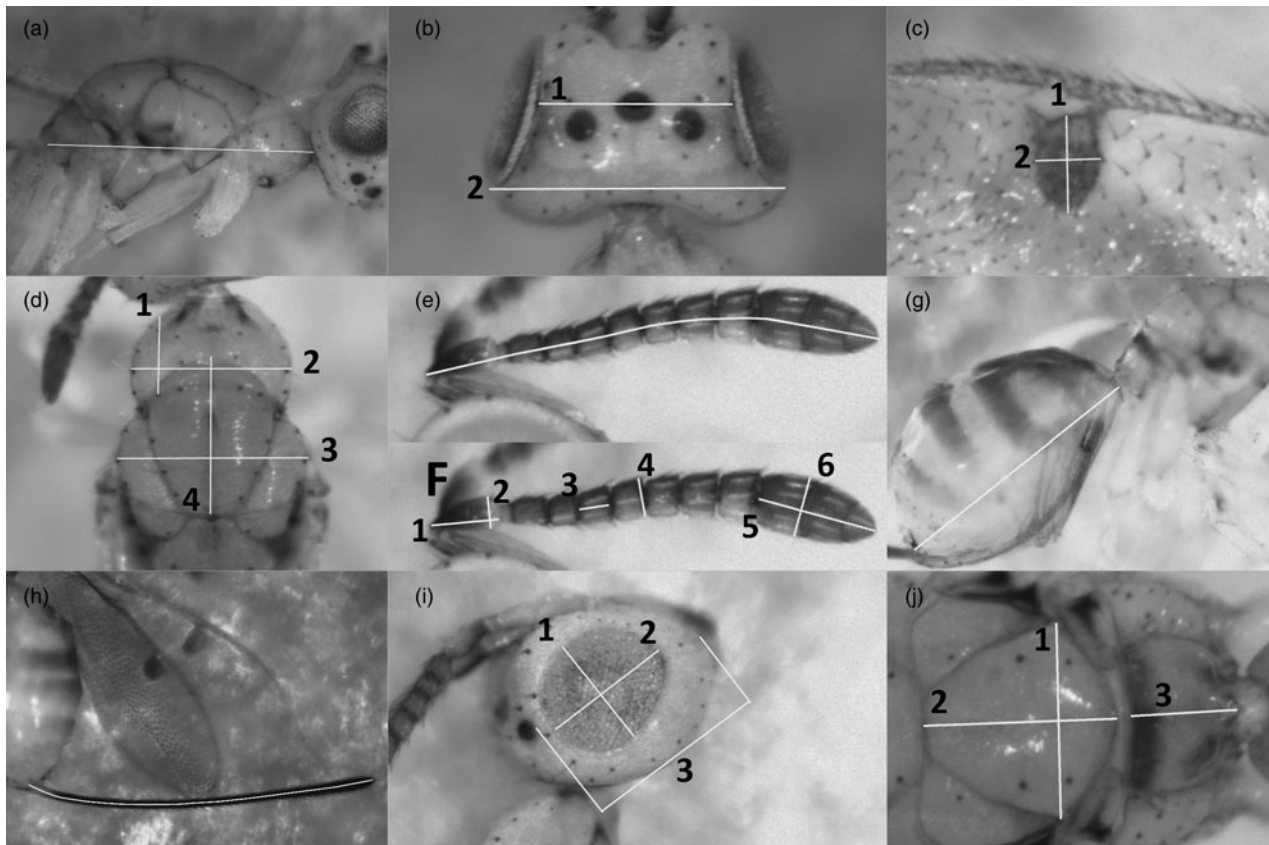
Figure 1. Measurement of body characters. (a) *mss.ll*; (b1-2): *eye.d, head.b*; (c1-2): *stg.l, stg.b*; (d1-2-3-4): *pnc.l, pnc.b, msc.b, msc.l*; (e) *pdl.flg; F1-2-3-4-5-6: ped.l, ped.b, fu3.l, fu4.b* (drawn as example, similarly measured for other funicle segments), *clv.l, clv.b*; (g) *gst.ll*; (h) *ovi.l*; (i1-2-3): *eye.b, eye.h, hea.hl*; (j1-2-3): *sct.b, sct.l, ppd.l*.

(Bioline, Eveleigh NSW, AUS). Total reaction volumes were 10 μl including DNA template (1 μl), primer (1 μl each, at 10 μM concentration), premixed 5× buffer (2 μl), HSTaq DNA polymerase (0.1 μl), and H_2O (4.9 μl). PCR thermo-cycling in a Bio-Rad T100 (Greenslopes, QLD, AUS): 95°C, 1 min + 35 cycles of (95°C, 1 min + 55°C, 1 min + 72°C, 1 min) + 72°C, 5 min final extension then holding at 10°C. When primer 1775-COI-F was used, the annealing temperature was reduced to 50°C.

DNA primers (table 2) followed previous work on *Megastigmus* (Scheffer and Grissell, 2003; Boivin *et al.*, 2014; Roques *et al.*, 2016) targeting the inner region of the mitochondrial gene cytochrome oxidase 1 (COI mtDNA) and nuclear fragment coding 28S rDNA, from the D1 to D3 region. Amplification was first attempted with primers 1775-COI-F/2773-COI-R (amplicon size 1040 bp) and 28S-D1F/28S-D3R (amplicon size c.a. 1090 bp) (Boivin *et al.*, 2014; Roques *et al.*, 2016). The alternative combination 28S-D1F/28S-1059R (amplicon size c.a. 1080 bp) was used to amplify the 28S fragment when necessary. For COI, because the primer 1775-COI-F co-amplified a pseudogene (nuclear copy of mitochondrial DNA, *numt*) in *M. zvimendeli*, the upstream forward primer LCO1490 (Folmer *et al.*, 1994) was alternatively used to amplify an extended fragment (amplicon size 1304 bp). Even in difficult cases, the reverse sequences 2773-COI-R successfully provided clean reading results covering the 1040 bp target region. For part of the dataset, the internal reverse primer 2399-COI-R resulted in a fully matched fragment of 904 bp extending from the middle of the target region to the

start of the barcoding fragment, allowing BLAST searches for matching partial barcode and subsequent analysis based on the barcoding region.

PCR products with a single band at the desired fragment size, visualized by electrophoresis on 1× TBE and agarose gel with GelRed® (Biotium, California, USA), were sent to Macrogen Inc. (Seoul, ROK) for purification and Sanger sequencing. For smaller batches (<10 samples), PCR products were purified on-site using ExoSAP-IT (Thermo Fisher Scientific, MA, USA). Sequencing reactions were conducted on-site using BigDye Terminator v3.1 Cycle Sequencing Kit (Thermo Fisher Scientific, MA, USA), and products were sent to the Australian Genome Research Facility (QLD, Australia) for sequencing.

Localities of analyzed *M. zvimendeli* and *M. manonae* in Australia, including the number of morphometric specimens, are illustrated in fig. 2.

DNA sequence analysis

Forward and reverse sequences were aligned and edited using Geneious 11.0.2 (Biomatters, Auckland, NZ). Primer sequences were removed, and alignments were trimmed to equal lengths (867 bp for 28S rDNA and 885 bp for COI mtDNA). Mitochondrial DNA was verified by translating the genetic code to amino acids using Geneious 11.0.2 to check for stop codons which suggested the presence of pseudogenes. Sequences from two specimens of *M. manonae* contained ambiguous sites,

Table 2. Names, sequences and reference sources of primers used for DNA extractions

Primer name	Sequence	Reference
1775-CO1-F (Forward)	CGAATAAATAATATAAGATTTTG	Scheffer and Grissell (2003)
LCO1490 (Forward)	GGTCAACAAATCATAAAGATATTGG	Folmer et al. (1994)
2399-CO1-R (Reverse)	TGTAGCTGAAGTAAAATAAGC	Self-designed
2773-CO1-R (Reverse)	GGATAATCTCTATATCGACGAGGTAT	Scheffer and Grissell (2003)
28S-D1F (Forward)	ACCCGCTGAATTTAAGCATAT	Auger-Rozenberg et al. (2006)
28S-D3R (Reverse)	TAGTTCACCATCTTTCGGGTC	Auger-Rozenberg et al. (2006)
28S-1059R (Reverse)	TTTCGGGTCCCAACGTGTAC	Self-designed

illustrated by double peaks nested within regions of clear, unambiguous signal, likely representing within-individual mitochondrial copy differences, so the sites were labelled with a degenerate base following the IUPAC ambiguity code.

Genetic distances and base compositions were calculated using MEGA X software (Kumar et al., 2018). Trees were constructed using Maximum Likelihood (ML) algorithm with the PHYML plugin (Guindon et al., 2010) in Geneious 11.0.2 (Biomatters, Auckland, NZ). For single-gene ML analysis, the optimal model of DNA evolution was determined using the Bayesian Information Criterion in the program Jmodeltest 2.1.0 (Darriba et al., 2012). Support values were calculated by bootstrap resampling 1000 times. The concatenated dataset was partitioned into four blocks (28S + CO1 separated into 1st, 2nd and 3rd codon position) in PartitionFinder 2.1.1 (Lanfear et al., 2016) and analysed to determine the best GTR model (Tavaré and Miura, 1986) for use in constructing a ML tree in RAxML 8.2.11 (Stamatakis, 2014). Support values were calculated using the RAxML's Boostraping algorithm with 1000 replicates.

DNA-based species delimitation was performed using the web version of the Automatic Barcode Gap Discovery (ABGD) tool (Puillandre et al., 2012). ABGD was applied to the trimmed, aligned 885 bp COI region (from 1798 to 2688 in reference to Drosphila yakuba mtDNA). Genetic distance was based on the KP80 model, a common parameter in mtDNA-based species delimitation (Boykin et al., 2012; Collins et al., 2012; Evans and Paulay, 2012).

Genbank searches for matching sequences were performed using the Geneious BLAST tool. Queries were representative sequences of M. manonae and M. zvimendeli corresponding to the barcode region and the Clyde-Bonnie region of the COI gene. The BLAST search returned two sequences (KF938926.1, JN559766.1) of 654 and 686 bp at the barcoding region and one sequence (KU984684.1, 417 bp) from the downstream end, that matched >99% with M. zvimendeli query sequences, with all other entries <93.2% (Supplementary Document 3). Trees containing Genbank-obtained sequences were built separately by alignment with the sequences generated in this study then trimmed to the reduced length of the Genbank sequences. The approximate fragment locations are presented in Supplementary Document 4.

Scanning electron microscopy

Representative specimens were dehydrated with hexamethyldisilazane (HMDS) and gold-coated using a Dynavac SC150 Sputter Coater (Dynavac High Vacuum Pty. Ltd., Victoria, Australia). Scanning electron microscope images were taken using a Hitachi Tabletop Microscope model TM-1000 (Hitachi High-Technologies Corporation, Tokyo, Japan).

Results

Multivariate ratio analysis of variation in body size and shape

Application of the function PCA ratio spectrum to all specimens as a single group identified principal components contributing to morphometric variations without prior species-determinant input. In shape space, PC1 and PC2 accounted for 50% of the variation of the entire sampled population. The first principal component is in congruent with the separation of species, although a clear cut between two clusters could not be established (fig. 3).

The PCA ratio spectrum (fig. 4) identified ool.l at the extreme high end, eye.h, eye.b and breadth of funicle segment fu2 to fu6 at the extreme low end. These characters, except fu2.b to fu6.b, were found to contribute to species discrimination. LDA ratio extractor identified eye.b/ool.l, fu1.l/stg.l and eye.h /fu2.l as the three best discriminating ratios. Combining the best two ratios successfully separated the studied species in a scatterplot (fig. 5). The calculated ratios for LDA-suggested characters (M. zvimendeli vs M. manonae, range 5th percentile–95th percentile) are: eye.b/ool.l (2.9–3.9) vs (4.3–6.4); stg.l/fu1.l (2.4–3.0) vs (3.0–3.7); eye.h/fu2.l (5.9–8.0) vs (7.9–10.0). This suggests that the two species can be separated when judgement is based on a series of individuals. Further, the calculated D.shape are much higher than D.size in all of the three best discriminative ratios, indicating that species are mostly separated by differences in the shape of characters (Supplementary Document 5).

Molecular species delimitation

Sequences of nuclear DNA coding partial 28S rRNA were obtained for M. manonae (13 specimens) M. zvimendeli (19 specimens) and M. pretorianensis (4 specimens), all trimmed to 867 bp. Guanine and cytosine accounted for 57.5% of the total bases on average, illustrating a slight GC bias. Within the studied group, nuclear 28S DNA sequences were highly conserved: intraspecific pairwise differences were 0% in all three species, maximum interspecific divergence was 1% (8 bases).

Partial mitochondrial DNA coding COI were sequenced and trimmed to 885 bp for 18, 13 and 4 specimens of M. zvimendeli, M. manonae and M. pretorianensis, respectively. The sequences contained 74.6% adenine and thymine, demonstrating a strong AT bias as in previous hymenopteran mtDNA studies (Castro
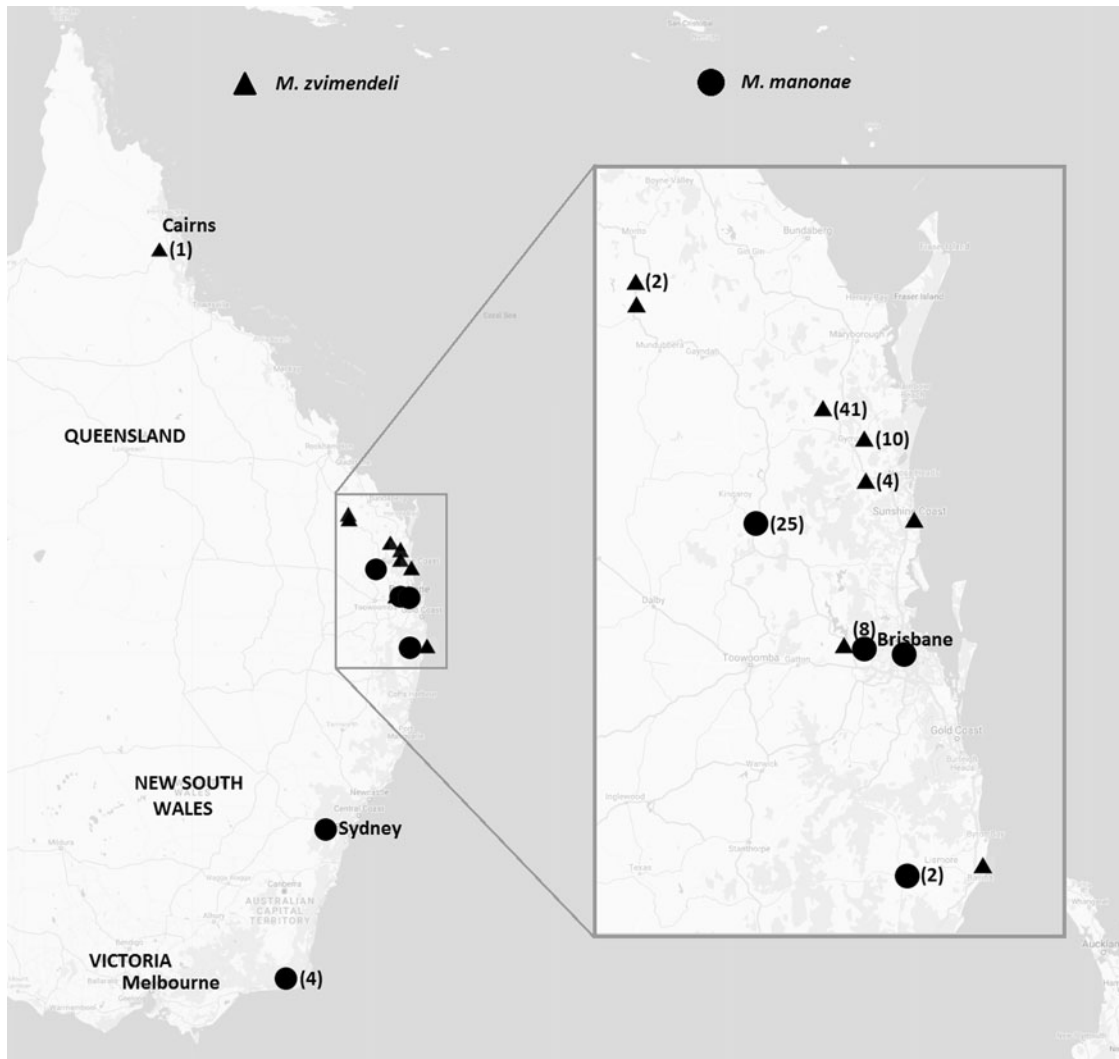
Figure 2. Distribution of Australian specimens of *Megastigmus zvimendeli* (triangles) and *M. manonae* (circles) used in the study. Numbers indicate morphometric samples in each location. Species identity was confirmed by DNA sequences of representative samples from all localities.

et al., 2002; Rokas *et al.*, 2002). Thymine alone accounted for 46.1–46.8% of the total number of bases in the coding strands. COI sequences of *M. manonae* (maximum 2.3% intraspecific difference) were more divergent than those of *M. zvimendeli* (maximum 0.3% intraspecific difference).

The generated sequences, including those of the outgroup (*M. zebrinus*) have been submitted to Genbank (Accession number MN165877 to MN165951).

Application of the ABGD tool to the aligned 885 bp COI sequences (Supplementary Document 6) revealed a clear barcode gap between KP80 distance of 0.02 and 0.06, which respectively represented the maximum intraspecific and minimum interspecific distances. DNA sequences were firmly assigned to four groups (*M. zvimendeli*, *M. manonae*, *M. pretorianensis* and the outgroup *M. zebrinus*). Specimens identified as *M. zvimendeli* from Kenya and Israel, and a specimen identified as *M. sichuanensis*, were also placed within the *M. zvimendeli* group.

The program PartitionFinder 2.1.1 recommended the models GTR + G, GTR + I + G, GTR and GTR + G for the 28S and the 1st, 2nd and 3rd codon position, respectively. The model GTR + G represented most of the variation (28S and the 3rd

codon position of COI) in the partitioned concatenated dataset and was therefore selected for phylogeny reconstruction in RAxML (Stamatakis, 2014). The reconstructed phylogeny was congruent with the ABGD species assignment, with bootstrap support from 90 to 100% (fig. 6a). The ABGD and ML analyses assigned a specimen from NSW-Australia with *M. pretorianensis* from South Africa, which was then verified using diagnostic characters (Doğanlar, 2015), confirming the presence of *M. pretorianensis* in Australia. The Australian *M. pretorianensis* specimens were from a local gall-inducing *Leptocybe* sp. that differs from the two invasive *Leptocybe* spp. in COI sequence (Le *et al.*, unpublished).

Before analysis of Genbank sequences, 13 and 21 bases were respectively removed from the downstream ends of KF938926.1 and JN559766.1 due to overlap with primer region, and a strong indication of technical misread commonly found in Sanger sequencing, illustrated in a disproportionately high ratio of mismatch of this region to published congeneric sequences. Sequences were subsequently aligned to available data and trimmed to the same length for tree construction and distance calculation. KP80 distance (≤0.8%) and ML inference (fig. 6b, c)
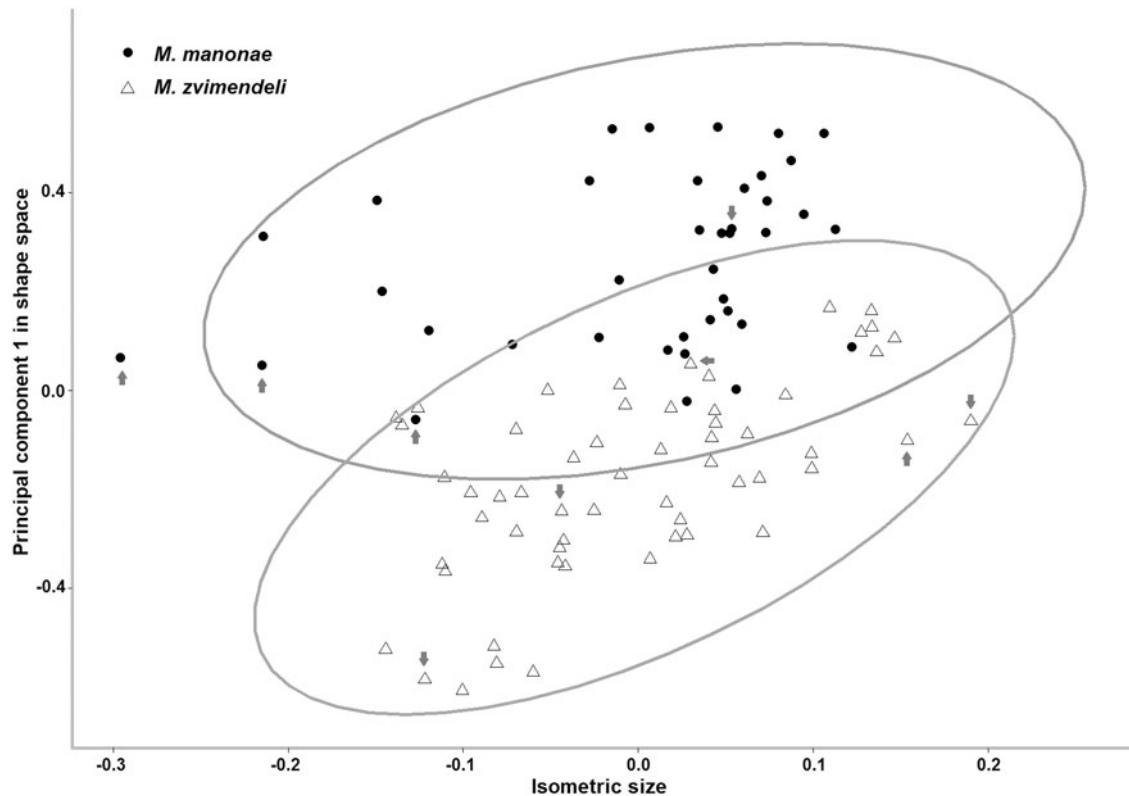
Figure 3. Scatterplot of isometric size against PC1 in shape space. Specimens confirmed by COI DNA sequence were marked with arrows. Confidence ellipses assuming multivariate normal distribution.

confidently confirmed that the Genbank sequences and Australian *M. zvimendeli* are the same species.

Species description

Megastigmus manonae sp. nov.
(figs 7 and 8).

Type material

Holotype: [-26.653896, 151.956021 / D'Anguilar Hwy, near Parsons Rd / Nanango Queensland 4615] // [HOLOTYPE ♀ / *Megastigmus manonae*] Queensland Museum (QM) South Brisbane, QLD, Australia. Reg. No. T245894, 1♀; card mounted; emerged from *Leptocybe* spp. gall on roadside *Eucalyptus tereticornis;* collected 16.i.2018.

Paratypes: Same data as holotype: QM 7♀, 4♂; Australian National Insect Collection, Black Mountain (ANIC), Black Mountain, ACT, Australia 7♀, 3♂ (ANIC 32-141414 to 23); Queensland Department of Primary Industries Insect Collection (QDPC), Dutton Park, QLD, Australia: 7♀, 2♂ (QDPC-0 −176208 to 176216).

[-27.487666, 152.662933 / Fairneyview – Fernvale Rd, / Fairney View QLD 4306], Australia; QM 3♀, 3♂; ANIC 2♀, 2♂ (ANIC 32-141424 to 141427); QDPC: 3♀, 1♂ (QDPC-0 −176208 to 176216); card mounted; emerged from *Leptocybe* galls on roadside saplings of *Eucalyptus tereticornis*; collected 17.xi.2017.

[-28.818824, 153.080054 / Manifold Rd, N. Casino NSW 2470], Australia; QM, 1♀; card mounted; emerged from *Leptocybe* galls on roadside saplings of *Eucalyptus* sp.; collected 14.xii.2018.

Same collection data as holotype: QM: 3♂, 3♀; HMDS treated, sputter coated, mounted on one metal stub for SEM.

Etymology

The specific epithet *manonae* (a noun in the genitive case) is named after Dr Manon Griffiths, an entomologist and NHL's supervisor who sadly passed away during the preparation of this manuscript.

Description

Diagnosis: 1. small, *gst.ll* + *mss.ll* <1.4 mm, with 2 pairs of scutellar setae, the anterior pair inserts at the approximate level of the posteriormost point of axilla and much longer than the posterior pair; 2. body darkly pigmented, most conspicuous in male: lightest male form having dark black colour on vertex, propodeum, anterior edge of mesoscutal midlobe and anterior half of tergites; darkest male form with scutellum and mesoscutal midlobe entirely black; 3. female eyes large from a lateral view, making up 80% length from vertex to mouth margin, *fu3* not shorter than *fu2*.

Female. Colour and colour variation: Body ranging from dominantly yellow to almost black to unassisted eyes. Colour variation most readily observed in mesosoma; the lightest form having notauli, scutoscutellar suture and anterior edge of mesoscutal midlobe black; the darkest form with scattered black pigments, making mesoscutum superficially black. Face and vertex from yellowish orange to whitish-yellow. Eye reddish. Occiput, mandibles and eye margin black. Pedicel and flagellum dark brown from dorsal view to yellowish-orange from ventral view; scape and pedicel much darker dorsally than ventrally. The lateral panel of pronotum, mesopleuron, prepectal shelves and prostenum dark yellow to dominantly black. Pronotal collar from
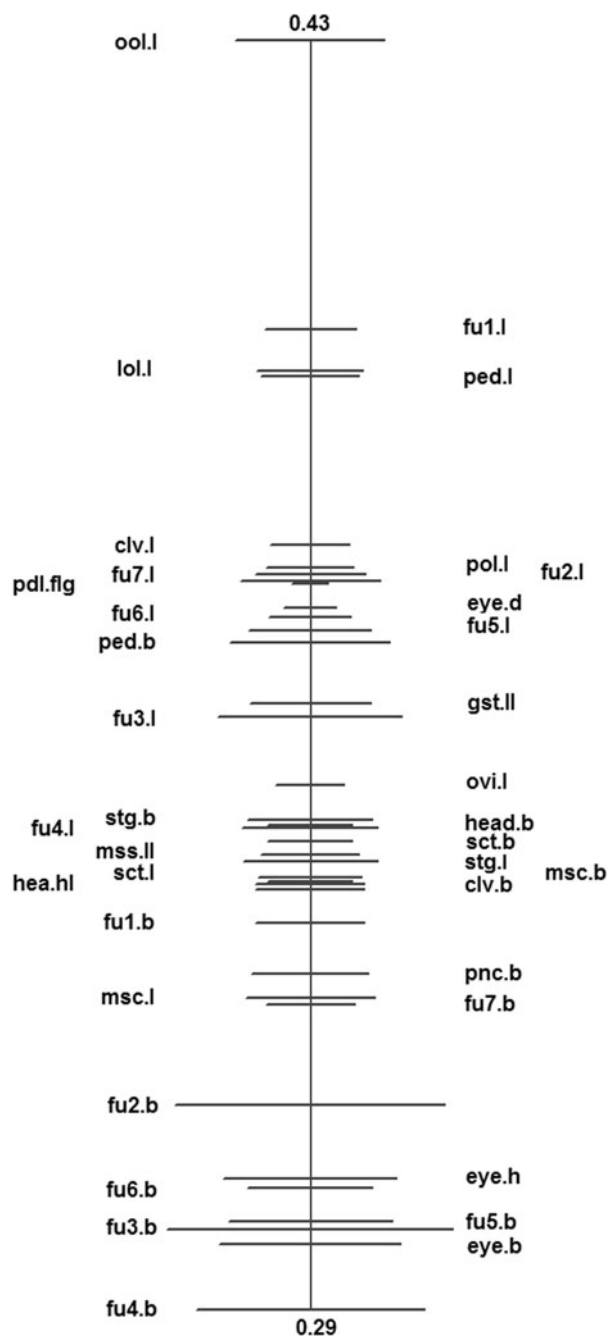
Figure 4. PCA Ratio Spectrum of the first principal component in shape space. Horizontal bars show 68% bootstrapping confidence intervals. Characters at two extreme ends explain most of variation in the first principal component.

concolourous to strongly paler than mesoscutum. Anterior of abdominal sclerites each with an anteriorly darkened band, grey to black, becoming orange or yellow posteriorly except the median of first and second tergites. Ovipositor sheaths black. Ovipositor stylets copper yellow.

Head. Head shape from lateral view cuneate (fig. 7j). Eye large, from lateral view making 80% dorsoventral length from vertex to mouth margin (*eye.h*/*hea.hl* 0.72–0.86 in morphometric specimens), surrounded by a ring of setae along the margin. Head breadth at posterior eye margin 0.30–0.45 mm. Ratio *head.b*/ *pol.l* 2.8–3.7, *head.b*/*eye.d* 1.5–1.8, *pol.l*/*ool.l* 2.5–3.9. Lower face

with striae convex towards mandibles. Antenna clavate; funicle and clava segments with one row of sensilla. Scape reaching the level of ocelli. Ratio *pdc.flg*/*head.b* 1.1–1.3. Pedicel significantly longer and wider than *fu1* (*ped.l*/*fu1.l* 1.6–2.4). Funicles subequal in length (*fu1.l > fu3.l > fu2.l* with few exceptions), widened from *fu1* to *fu7* (*fu1.b*/*fu7.b* 0.5–0.7), hence segments appear transverse except first and second funicle nearly cylindrical. Club length varied (*clv.l*/*fu7.l* 2.7 −3.7).

Mesosoma: approximate length of gaster (*mss.ll*/*gst.ll* 0.8–1.2), *mss.ll*/*msc.b* 1.6–2.0, *msc.b*/*head.b* 0.8–1.1. Pronotum posteriorly overlaps but not completely concealing the concave anterior edge of mesoscutal midlobe. From dorsal view, pronotal collar sub-rectangular, twice as broad as length (*pnc.l*/*pnc.b* 0.4–0.6). Pronotal collar setae from dorsal view: two longitudinal rows near lateral edges, sparse long setae nearly forming two submedian longitudinal rows, a transverse row at posterior edge. Mesoscutal midlobe and scutellum with fine transverse, sometimes inconspicuous sculpture. Frenal groove absent, frenum indistinct. Dorsellum conspicuous, paler than two lateral panels of metanotum, the lateral panels frequently with a brighter posterior region forming a transverse, near-oval shape at each panel. Propodeum slightly reticulated, more densely and hence appears punctate between two plicae. Propodeal callus with a patch of hairs paler than body setae. Legs white except tarsal claws dark and hind coxa brownish, darker basally. Forewing (fig. 7g) hyaline, stigma darkened brown. Basal setal line incomplete. Cubital fold conspicuous. Submarginal vein (*smv*) with 6–7 setae, narrower than parastigmal vein (*pv*) and post marginal vein (*pmv*). *Smv* length approximate (*pv* + *pmv*). *Pmv* forms an acute angle with and approximates the length of stigmal vein. Upper part of stigma vein (stigma petiole) short, slightly longer than uncus, stigma knob length approximately 1.5 × breadth (*stg.l*/*stg.b* 1.4–1.7).

Metasoma: inconspicuous petiole, hence gaster rather sessile. Tergites from dorsal view with a ring of black setae at posterior edges. Ratio *ovi.l*/*gst.ll* 1.4–2.0.

Male. Body smaller than females (paratypes, *mss.ll* + *gst.l* 1.0–1.3 mm); body colour (fig. 7c and h) as in diagnosis character, usually darker than females. Head: head and antennal shape similar to females, a lower face from lateral and frontal view paler than mesoscutum, vertex with a black butterfly-shaped region covering ocelli; *ool.l* short. Eye reddish with black margin surrounded by a ring of black setae like in females. Antennal segments paler ventrally than from dorsal view. Size (paratypes, mm): *head.b* 0.33–0.42, *eye.d* 0.2–0.25. ratio: *pol.l*/*ool.l* 3.4–4.4, *pol.l*/*lol.l* 2.2–2.3, *head.b*/*eye.d* 1.6–1.7, *eye.d*/*pol.l* 1.7–2.0, *ped.l*/*fu1.l* 1.6–2.2. Mesosoma: shape of mesosoma, mesoscutum and scutellum like in females. The transverse sculpture on mesoscutal midlobe usually conspicuous, most noticeable on darker specimens. Scutellum sometimes appears punctate in lighter forms. Scutellum with 1 additional pair of scutellar setae in addition to the characteristic two pairs. Pronotum shape like in females, paler than mesonotum form dorsal view, concolourous to lower face. Legs generally whitish to yellow, darker at tarsal claws. Stigma knob with a clear margin like in females but less elongated. Length and breadth of the uncus and stigma petiole vary. Size: *mss.ll* 0.5–0.7, *msc.b* 0.3–0.4; Ratio: *stg.l*/*stg.b* 1.2–1.4, *mss.ll*/*msc.b* 1.7–2.0, *msc.b*/*head.b* 0.9. Metasoma usually much smaller than mesosoma, *gst.ll* 0.5–0.6 mm with the first tergite elongated, petiolate.
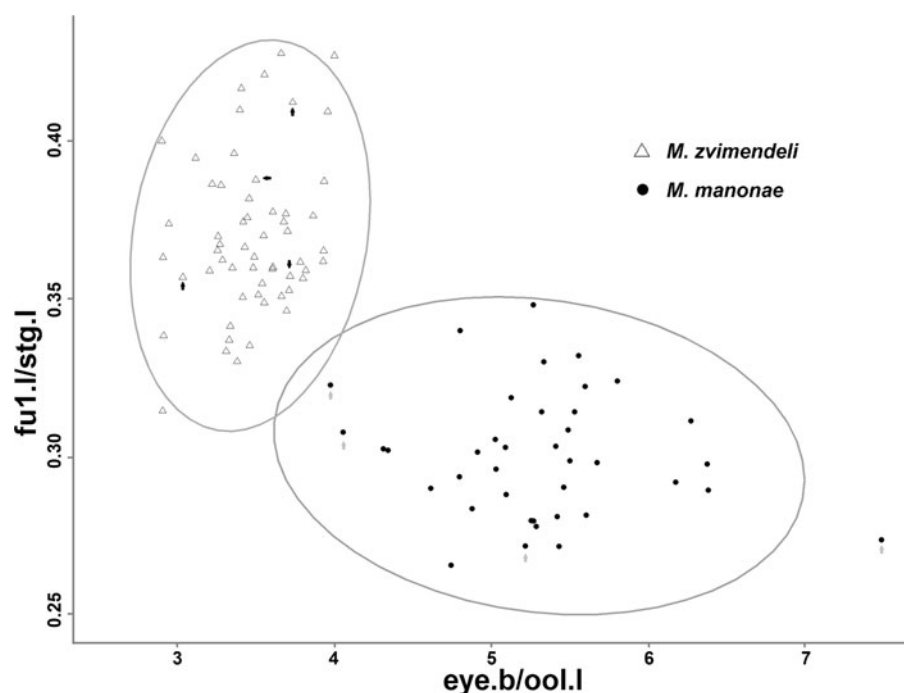
Figure 5. Scatterplots illustrating discrimination of *M. manonae* and *M. zvimendeli* with two best discriminating ratios selected by LDA Ratio Extractor (*eye.b/ool.l* vs *fu1.l/stg.l*). Dots pointed with arrows denote specimens confirmed by COI DNA sequence. Confidence ellipses were based on an assumed multivariate normal distribution.

Biology

Megastigmus manonae emerged from *Leptocybe* spp. galls on *Eucalyptus tereticornis* seedlings and from a small blister, non *Leptocybe* spp. – induced galls on leaves of young *Eucalyptus* sp. Females that emerged from field-collected *Leptocybe* spp. galls oviposited on laboratory-induced *Leptocybe* spp. galls and reproduced successfully. In laboratory condition, development time (from oviposition to emergence of the new generation) varied from 19 to 22 days and a maximum number of offspring was nine (NHL, pers. obs., four parental females).

Taxonomical Remarks

Megastigmus manonae grouped to *M. zvimendeli* and *M. pretorianensis* in a phylogenetic tree of eucalypt-associated *Megastigmus* with minute size, short and clavate antennae, ovipositor similar in relative length to mesosoma, similar forewing and stigma knobs shape, and two pairs of scutellar setae (Le *et al.*, unpublished). In Australia, emergence from the same collected material, collection site and eucalypt plant can include any of the combination of *M. manonae*, *M. zvimendeli*, *M. lawsoni* and an unidentified species (*Megastigmus* sp. 1). Small individuals of *Megastigmus* sp. 1 and *M. zvimendeli* are similar in size and body colour but males and females of *Megastigmus* sp. 1 can be distinguished from *M. zvimendeli* by their three pairs of black scutellar setae (fig. 9a). Males of *M. lawsoni* have a black patch on the mesonotum but the coloration is always confined to the median part of the transscutal articulation, never reaching the anterior edge of mesonotum (fig. 9c). This coloration delimits these species: the black patch is lacking in *M. zvimendeli*; while in *M. manonae* the black pigments are unconfined (fig. 7c and h). Females of *M. lawsoni* and *M. zvimendeli* have similar colour and shapes; rare cases of *M. lawsoni* females have four scutellar setae instead of the typical single pair as in Doğanlar and Hassan (2010). These two species can be misidentified without the presence of males, but *M. lawsoni* can be identified by longer stigma knobs and different, somewhat irregular placement of scutellar setae (fig. 9b and d).

Within the group of *M. zvimendeli*, *M. manonae* and *M. pretorianensis*, the first species can be identified by the dominantly yellowish-orange female colour, rarely with darkened notauli or scutoscutellar suture and never with black colour on the anterior edge of mesoscutum. *M. manonae* and *M. pretorianensis* both have darkly pigmented bodies, but *M. pretorianensis* appears closer to *M. zvimendeli* than to *M. manonae* in terms of body shapes: they can be separated by the same two best ratios that worked for *M. manonae* and *M. zvimendeli* (Supplementary Document 7). The ratio that could be most conveniently interpreted into body proportion is *eye.h/hea.hl*, representing the 'smaller eye' when observed from a lateral view. This ratio varied from 0.68 to 0.74 in 11 out of 12 measured *M. pretorianensis*, well within the 5th -95th percentile range of *M. zvimendeli* (0.64–0.76) and not exceeding that of *M. manonae* (0.74–0.85). In the study, *M. manonae* specimens with less conspicuously large eyes were further identified by having *fu3.l > fu2.l*. The *fu3* was significantly shorter for the Australian *M. pretorianensis* specimen (1♀ available for study), and the examined South African *M. pretorianensis* having *fu2* longer or at least subequal to *fu3*. For this reason, the character 'large eye' and *fu3.l ≥ fu2.l* were mentioned in the diagnosis of *M. manonae*. Additionally, *M. manonae* females usually have longer pronotal and mesoscutal setae which are much more conspicuous than that of *M. pretorianensis*.

Megastigmus pretorianensis was described with 'antennae inserted slightly above lower ocular line' (Doğanlar, 2015). We found this character highly subjective to observational error due to the generally low position of toruli in the studied group and the absence of an actual lower ocular line. This character was therefore disregarded for delimitation of *M. manonae* and *M. pretorianensis*. In addition, the breadth of funicle segments (*fu2.b* to *fu6.b*) were not selected by LDA Ratio Extractor despite being placed at the lower end of PCA spectrum. This indicates that the interspecific variation of funicle breadths for the two studied species were not strong enough to outweigh the intraspecific variation under the selected measurement technique. Removal of funicle breadths in fact improved the separation of two species
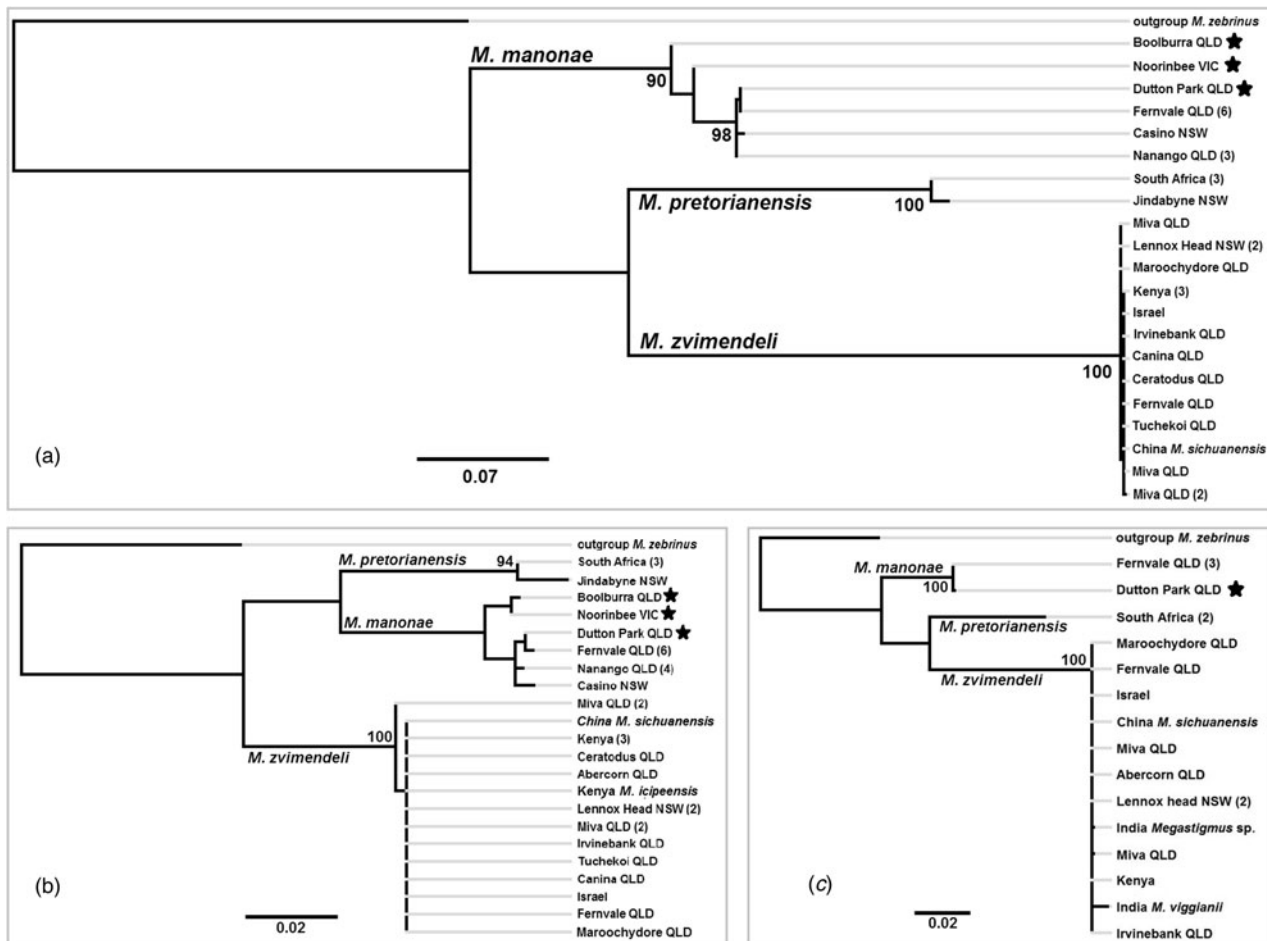
Figure 6. ML trees inferred from different DNA markers. (a) Phylogeny based on the concatenated COI + 28S sequences (867 + 885 bp), model of evolution (GTR + G), data partitioned into four blocks (28S + three COI codon positions) using RAxML. (b) Placement of the Genbank entry KU984684.1 (*M. icipeensis*, Kenya) based on COI downstream 417 bp sequences, model of evolution (TPM1uf + I), using PHYML. (c) Placement of the Genbank entry JN559766.1 (*M. viggianii*, India) and KF938926.1 (*Megastigmus* sp., India) based on 613 bp sequences at COI barcoding region, model of evolution (TIM3 + G), using PHYML. (b) and (c) are from non-overlapping regions. (GTR: Generalized time-reversible; TPM: 3-parameter model; TIM: Transitional model; uf: unequal base frequency; G: with gamma-distributed among-site rate variation; I: with a proportion of invariable sites). Outgroup specimen was *M. zebrinus* for all trees. Star-marked nodes are from non-*Leptocybe* galls. Numbers adjacent to nodes indicate bootstrap support ($n = 1000$; only values ≥80 are shown). Number of substitution rate categories = 4 for all PHYML analysis. One representative was selected for identical sequences from the same locality. Identical sequences from different localities and non-identical sequences from the same locality were retained in ML analysis.

(Supplementary Document 8). Funicle breadths together represent the thinness of flagellum and consequently the differently perceived length of the antenna (Supplementary Document 9), which should be considered if species identification is based on few specimens.

Megastigmus zvimendeli Doğanlar & Hassan 2013

(figs 10 and 11). Description and diagnostic characters of *M. zvimendeli* were provided by Doğanlar (2015), Doğanlar and Hassan (2010), and Roques *et al.* (2016, as *M. icipeensis*) (Roques *et al.*, 2016). We provide additional data on sizes and diagnostic characters of female specimens, and comments on synonymies and possible misidentification.

Synonyms

Megastigmus icipeensis Roques & Copeland, 2016. Syn. n.
Megastigmus sichuanensis Doğanlar & Zheng 2017. Syn. n.
Megastigmus judikingae Doğanlar & Hassan 2010. Syn. n.. Sizes (Australian morphometric specimens, mm): *head.b* 0.3–0.4; *hea.hl* 0.2–0.3; *eye.h* 0.15–0.21; *eye.b* 0.12–0.15; *pdl.fgl* 0.4–0.6;

eye.d 0.21–0.26; *mss.ll* 0.5–0.7; *msc.b* 0.3–0.4; *gst.ll + mss.ll* 0.9–1.5; *ovi.l* 0.8–1.3; Ratio: *eye.b/ool.l* 2.6–4.0; *pol.l/ool.l* 2.0–3.1; *ped.l/fu1.l* 1.5–2.3; *fu1.b/fu7.b* 0.5–0.7; *eye.h/fu2.l* 5.7–8.0; *stg.l/fu1.l* 2.3–3.2; *fu1.l/fu7.l* 0.8–1.2; *msc.b /head.b* 0.8–1.0; *mss.ll/msc.b* 1.5–2.1; *stg.l/stg.b* 1.3–1.7; *ovi.l/gst.ll* 1.4–2.1; (*gas.ll + mss.ll)/ovi.l* 1.0–1.3.

Diagnosis (females). 1. Scutellum with two pairs of setae, the anterior pair longer, inserting at the approximate level of the posterior-most point of axilla; 2. body almost concolourous orange; both male and female with mesoscutum and scutellum entirely concolourous yellowish-orange from dorsal view; darkest male body dominantly yellowish-orange mesonotum with narrow black scutoscutellar suture; pilosity of thorax mostly pale; 3. female eyes small, making up 65–75% of the head height from lateral view.

Taxonomical Remarks

Megastigmus judikingae and *M. zvimendeli* were distinguished by size and ratio of body characters in the original description
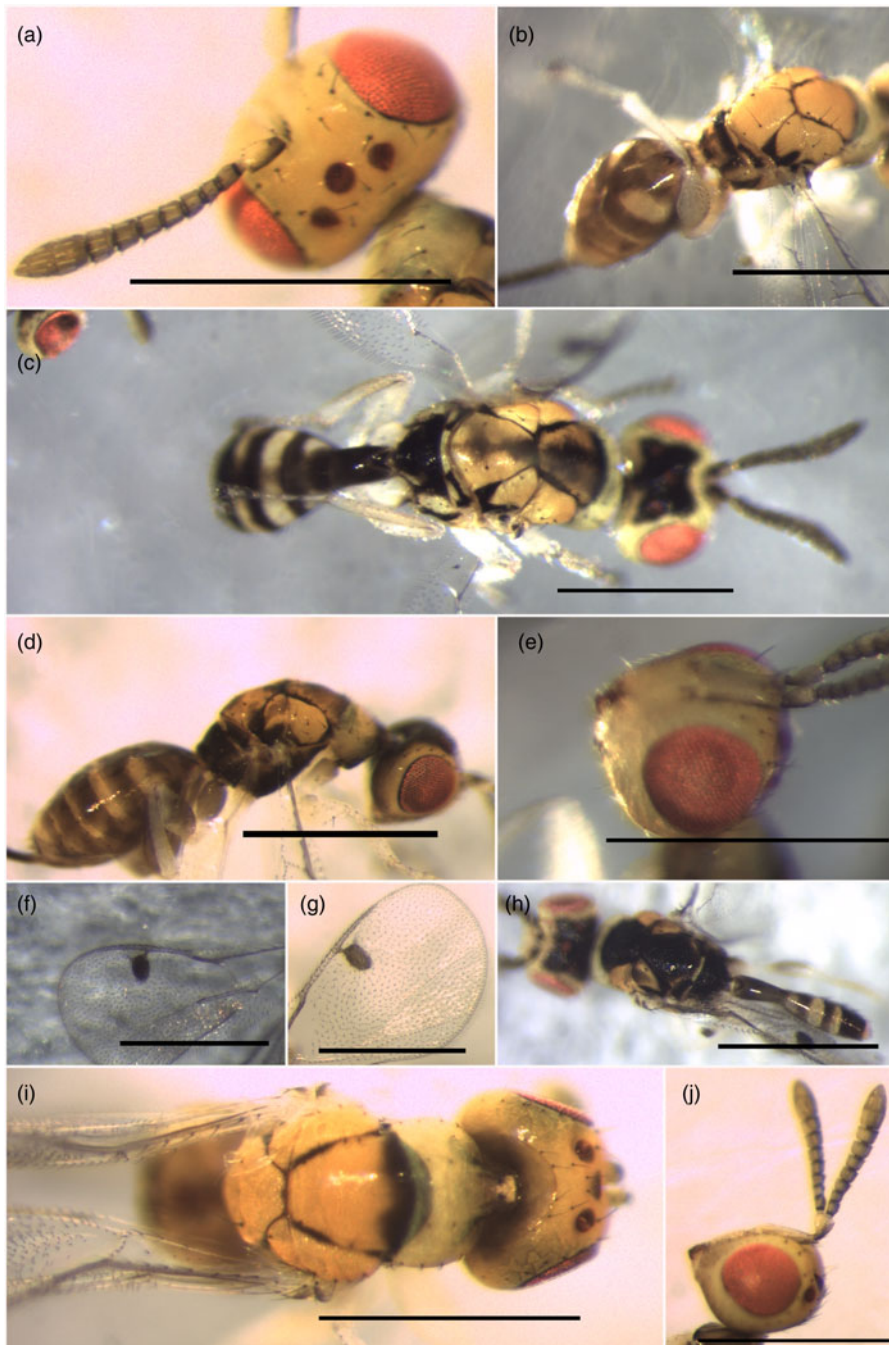
Figure 7. *Megastigmus manonae* (scale bars = 0.5 mm). Female: (a). pedicel and flagellum; (b, d): light form and dark form, dorsolateral view; (e) face showing toruli position; (g) forewing stigma; (i) mesoscutal midlobe, pronotal collar and occiput; (j) head and antenna from lateral view. Male: (c, h): light and dark form, dorsal view; (f) forewing stigma.

(Doğanlar and Hassan, 2010; Doğanlar, 2015). Synonymy of *M. zvimendeli* and *M. judikingae* is based on the observations below:

- Remeasurement of paratypes of *M. judikingae* (2♀, ANIC 111465, ANIC111466) based on characters delimiting *M. judikingae* and *M. zvimendeli* in the original paper (Doğanlar and Hassan, 2010) (*ped.l/fu1.l* 1.9–2.0, *fu1.b/fu7.b* 0.6–0.7; *combined length of funicle 5, 6, 7/clv.l* 1.1; *ovi.l/gst.ll* 1.6 to 1.8) varied within intra-species limit of *M. zvimendeli*. PCA clustering and ratio-based scatterplot comfortably placed the two paratype specimens into *M. zvimendeli* group (Supplementary Document 10).
- Labels on abovementioned paratypes record *E. tereticornis* as the host plant, rather than *Corymbia tessellaris* as in the original publication. *E. tereticornis* is a common host of *Leptocybe*-associated

M. zvimendeli, whereas *C. tessellaris* does not support *Leptocybe* development (Phạm *et al.*, 2009).
- These specimens and *M. zvimendeli* shared key characters of body size, body colour, scutellar setae position and colour, and placement of toruli.

Because the name *M. zvimendeli* has been cited in publications regarding the species' use in biocontrol (Dittrich-Schröder *et al.*, 2014; Bush *et al.*, 2017; Mendel *et al.*, 2017), precedence was given to *M. zvimendeli* Doğanlar and Hassan 2013 (the Principle of the First Reviser, Article 24.2, ICZN Code). *Megastigmus judikingae* Doğanlar and Hassan 2010 becomes a junior synonym.
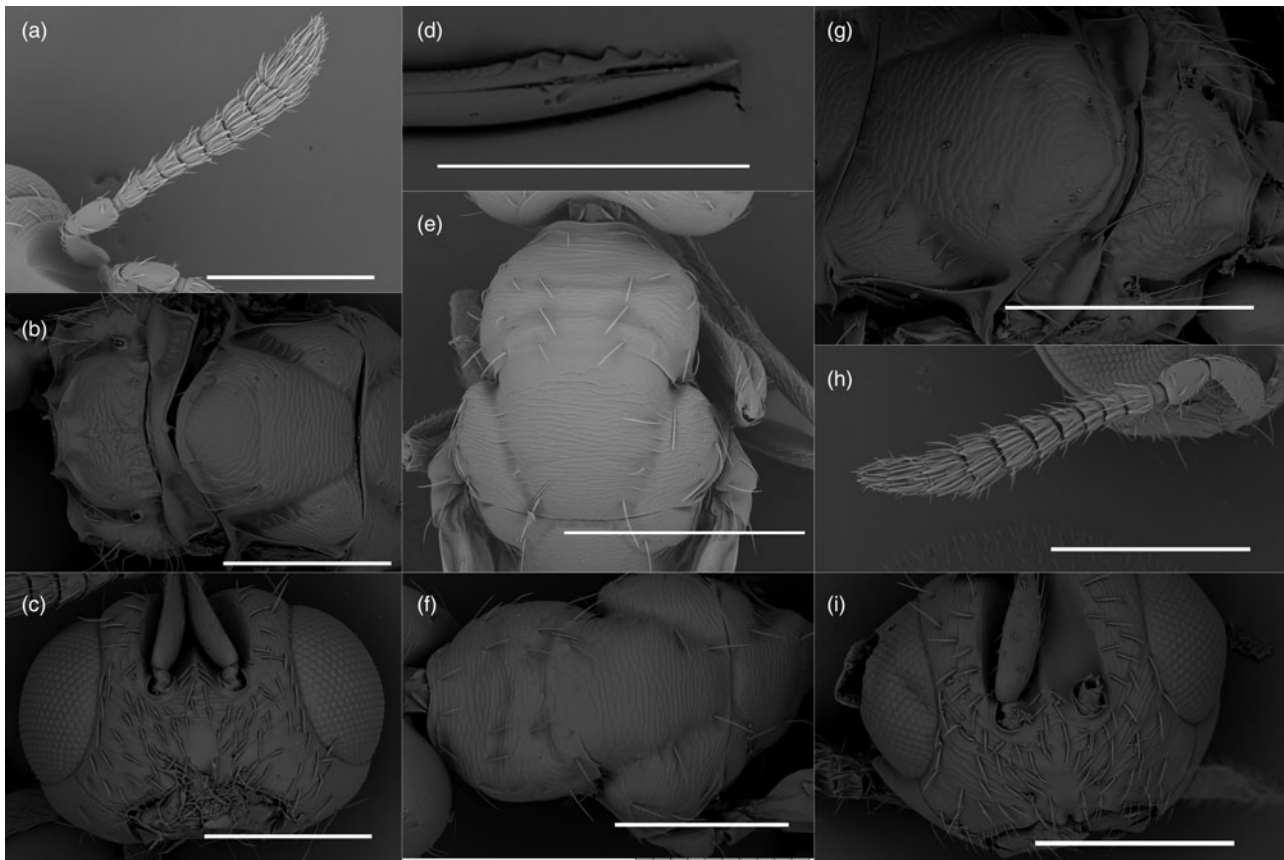
Figure 8. SEM photographs of *Megastigmus manonae*. Female: (a) pedicel and flagellum; (b) scutellum and propodeum; (c) toruli and scrobal depression; (d) drilling tip of ovipositor stylet; (e) pronotum and mesoscutum. Male: (f) pronotum and mesoscutum; (g) scutellum and propodeum; (h) pedicel and flagellum; (i) toruli and scrobal depression. Scale bars: a, b, c, f, g, h, i = 0.2 mm; d = 0.1 mm; e = 0.3 mm.

Megastigmus icipeensis Roques & Copeland was described in 2016 (Roques *et al.*, 2016) from Malaise trapped Kenyan specimens. The available COI DNA sequence from these specimens fully grouped with Australian *M. zvimendeli* and with *Leptocybe invasa*-associated *Megastigmus* specimens sent from Kenya by our colleagues and subsequently identified as *M. zvimendeli* (fig. 6). Characters including the minute size, distinctive orange body colour and pale bristles fully matched with *M. zvimendeli*. We, therefore, treat *M. icipeensis* Roques & Copeland 2016 as a junior synonym (Article 23. Principle of Priority, ICZN Code).

Megastigmus sichuanensis Doğanlar & Zheng was described in 2017 (Doğanlar *et al.*, 2017; Huang *et al.*, 2017). Nuclear 28S DNA and mitochondrial COI DNA sequences obtained from specimens provided by our colleagues in China fully matched *M. zvimendeli* (fig. 6). As in *M. judikingae*, the sizes (*ovi.l* 1.2 mm), body ratios (*mesosoma length/msc.b* 2.1, *clv.l/clv.b* 1.85, *stg.l/stg.b* 1.4) fell within the variation range of *M. zvimendeli* in our study. The number of scutellar setae, body and pilosity colour matched diagnostic characters of *M. zvimendeli*. We, therefore, synonymize *M. sichuanensis* and *M. zvimendeli*, with the latter name having precedence (Article 23. Principle of Priority, ICZN Code).

Megastigmus viggianii Narendran & Sureshan was described from specimens collected from the Indian Ukshi plant *Calycopteris floribunda* (Narendran and Sureshan, 1988) and linked with *Leptocybe* in subsequent studies (see Huang *et al.*, 2018; Le *et al.*, 2018). KP80 distance and phylogenetic analysis firmly placed two Genbank entries, JN559766.1 (recorded as *M. viggianii*) and KF938926.1 (unidentified *Megastigmus,* India), into the *M. zvimendeli* group. *M. viggianii* is described as of significantly larger body size (1.67–2.13 mm), distinct malar sulcus, all funicles elongated, and smooth frenum (Narendran and Sureshan, 1988). The examined holotype (Reg. No. T57893, donated to QM by Narendran in 1999 (Wright, 2019, pers. comm.) bears three pairs of scutellar setae, elongated funicles, and toruli at higher than the lower eye margin. These characters are not observed in *M. zvimendeli*; therefore, we believe JN559766.1 was misidentified. *Megastigmus viggianii* and *M. zvimendeli* remain two valid species, but with no association between *M. viggianii* and *Leptocybe* or eucalypts.

Discussion

Within *Megastigmus*, Bouček (1988) suggested the divergence of a distinctive entomophagous group with small size, low antennal sockets, convex lower face, short antennae and similarities in male and female antennal form. *Megastigmus* associated with *Leptocybe* galls in our study also differs from phytophagous species in minute sizes and distinctly clavate antenna in males and females. While phylogenetic relationships among them and their phytophagous congeners await elucidation, their size and morphological variation have confused researchers attempting morphological classification.

Our study successfully utilized morphometric and genetic data to discriminate two closely related species: *M. manonae,* sp. nov.,
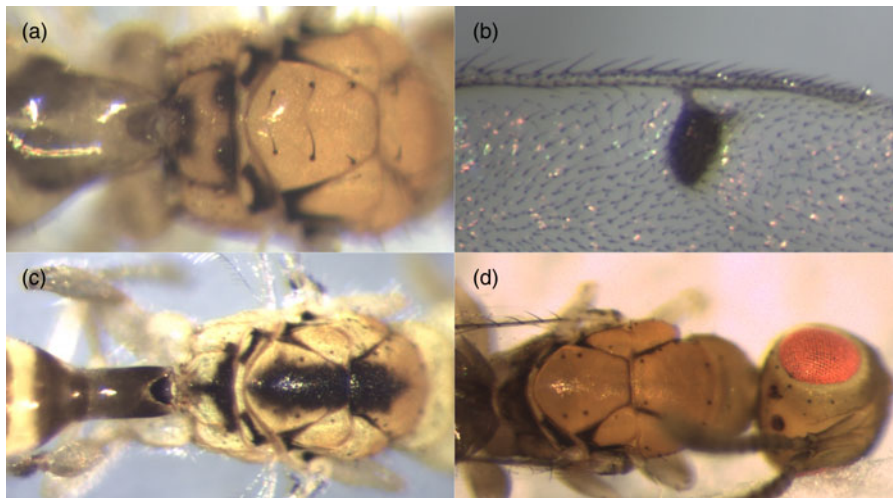
Figure 9. Possible misleading forms of Australian species that can be misidentified for *Megastigmus manonae* and *M. zvimendeli*. (a) scutellar setae, female *Megastigmus* sp. 1; (b) female stigma, *M. lawsoni*; (c) mesonotum colouration, male *M. lawsoni*; (d) scutellar setae, female *M. lawsoni*.

Figure 10. *Megastigmus zvimendeli* (scale bars = 0.5 mm). Male: (a) vertex and ocelli; (b) mesoscutal midlobe and pronotum; (c) forewing stigma; (d) abdomen. Female: (e) forewing stigma; (f) scutellum and propodeum; (g) mesoscutal midlobe and pronotum; (h) dorsolateral habitus; (i) head from lateral view; (j) vertex and ocelli.
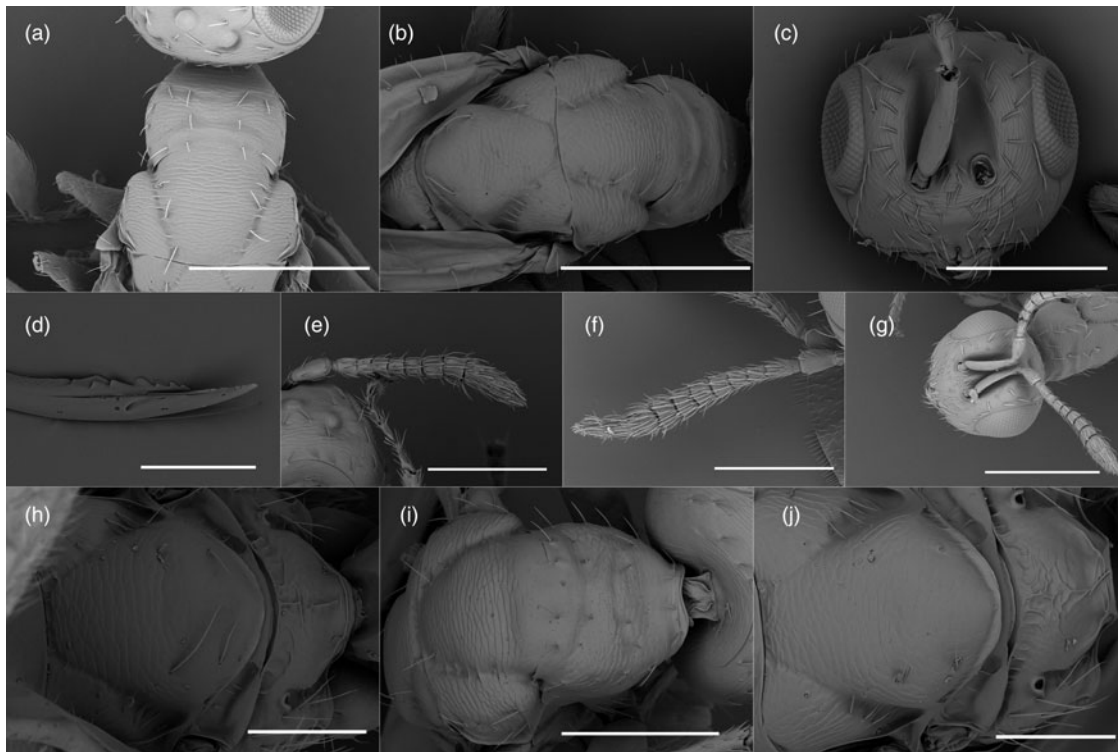
Figure 11. SEM photographs of *Megastigmus zvimendeli*. Male: (a) mesoscutal midlobe; (b) mesoscutum from dorsal view; (c) face, scape and toruli; (f) flagellum; (j) scutellum and propodeum. Female: (d) drilling tip of ovipositor stylet; (e) scape and flagellum; (g) face, scape and toruli; (h) scutellum and propodeum; (i) mesoscutal midlobe. Scale bars: a, b, g = 0.3 mm; c, e, f, i = 0.2 mm; h, j = 0.1 mm; d = 0.05 mm.

and *M. zvimendeli*. Key morphological characters contributing to variation among all specimens (*ool.l, eye.h, eye.b, fu1.l, fu2.l* and *stg.l*) were revealed by MRA. Moreover, the two species could not be separated by ratios involving funicle breadths and several body characters which are relied on in current taxonomic keys to parasitic *Megastigmus,* e.g. *pdc.fgl, clv.l, ovi.l*. This reiterates the need for exhaustive examination (Bouček, 1988; Auger-Rozenberg *et al.,* 2006; Protasov *et al.,* 2008). In addition, phylogenetic analyses revealed greater genetic diversity within *M. manonae* than *M. zvimendeli*.

The generated knowledge of morphological variation and complementary DNA data resulted in the synonymies of *M. zvimendeli* with *M. judikingae, M. sichuanensis* and *M. icipeensis*, and the disassociation of *M. viggiannii* as a *Leptocybe*-eucalypt gall associate. In turn, this illustrates the successful spread and establishment of *M. zvimendeli*, an Australian endemic parasitoid, in the invasive range of *Leptocybe* spp., unveiling the previously under-recognized success of this species in biocontrol. The findings also emphasize the need for coordinated examination and possible revision of *Megastigmus* spp. from *Leptocybe* galls worldwide. Gall-inducing insects are highly specialized (Price, 2005) and arose from evolutionary pathways starting from plant tissue miners or sedentary plant feeders (Price *et al.,* 1987). Considering the Australian origin of eucalypts, the long co-evolutionary history of insect-plant systems and the paucity of non-Australian entomophagous *Megastigmus*, a significant proportion of the purportedly fortuitous local *Megastigmus* spp. associated with *Leptocybe* spp. in their invasive range could have come from unintentional introductions from Australia. *Megastigmus pretorianensis*, which we confirmed present in

Australia and South Africa, is a tentative example requiring further specimens for an origin-tracing study.

Attention should be drawn to the co-occurrence of *Megastigmus* species in *Leptocybe* spp. galls. *Megastigmus zvimendeli* and *M. manonae* have been found in galls collected from the same location in Queensland (fig. 6a). Co-occurrence of *M. zvimendeli* with other *Megastigmus* species, even within the same gall, was observed frequently in collections (Le *et al.,* unpublished data). This could possibly be due to the multi-chambered, large *Leptocybe* galls being exploited at the same time by multiple parasitoids. Co-occurrence can confound identification and cause the unintended release of mixed species in biocontrol programs.

The conserved COI DNA sequences in *M. zvimendeli* precluded further population analysis of its worldwide movement, although its geographic origin is partly known through data on its discovery, collection and release. This high conservation is at odds with previous observations in which the rate of mutation in parasitic Hymenoptera is higher than that of nonparasitic insects (Castro *et al.,* 2002). Nevertheless, like Auger-Rozenberg *et al.* (2006) and Roques *et al.* (2016), we found DNA markers highly successful for *Megastigmus* species discrimination. Continued use of these markers will facilitate overall understanding of the genus and relationships between species that do and do not associate with eucalypts, from Australia and elsewhere, and phytophagous vs entomophagous species.

Like Borowiec *et al.* (2019), we have demonstrated the utility of morphological characters and molecular methods to discriminate species in cryptic eucalypt-gall associated wasps. While this successful combination of morphological and DNA tools will be applied to a broader range of endemic Australian *Megastigmus*

species (Le *et al.*, in prep), we recommend that non-Australian species unavailable for our study (e.g. *M. dharwadicus*, *M. thailandiensis*, *M. thithipornae*, *M. brasiliensis*, *M. leptocybus*) be examined in light of our findings. Understanding the status of *Megastigmus* species associated with *Leptocybe* will assist with identifying new biocontrol candidates and the potential host-switching and/or invasion processes that may underpin the diversity and distribution of eucalypt-associated *Megastigmus* worldwide.

References

Auger-Rozenberg MA, Kerdelhué C, Magnoux E, Turgeon J, Rasplus JY and Roques A (2006) Molecular phylogeny and evolution of host-plant use in conifer seed chalcids in the genus *Megastigmus* (Hymenoptera: Torymidae). *Systematic Entomology* **31**, 47–64.

Baur H and Leuenberger C (2011) Analysis of ratios in multivariate morphometry. *Systematic Biology* **60**, 813–825.

Baur H, Kranz-Baltensperger Y, Cruaud A, Rasplus JY, Timokhov AV and Gokhman VE (2014) Morphometric analysis and taxonomic revision of *Anisopteromalus* Ruschka (Hymenoptera: Chalcidoidea: Pteromalidae) – an integrative approach. *Systematic Entomology* **39**, 691–709.

Boivin T, Henri H, Vavre F, Gidoin C, Veber P, Candau JN, Magnoux E, Roques A and Auger-Rozenberg MA (2014) Epidemiology of asexuality induced by the endosymbiotic *Wolbachia* Across phytophagous wasp species: host plant specialization matters. *Molecular Ecology* **23**, 2362–2375.

Borowiec N, La Salle J, Brancaccio L, Thaon M, Warot S, Branco M, Ris N, Malausa J-C and Burks R (2019) *Ophelimus mediterraneus* sp. n. (Hymenoptera, Eulophidae): a new *Eucalyptus* Gall wasp in the Mediterranean region. *Bulletin of Entomological Research*, **109**, 678–694.

Bouček Z (1988) *Australasian Chalcidoidea (Hymenoptera). A Biosystematic Revision of Genera of Fourteen Families, with a Reclassification of Species.* Wallingford, UK: C.A.B International.

Boykin LM, Armstrong KF, Kubatko L and De Barro P (2012) Species delimitation and global biosecurity. *Evolutionary Bioinformatic Online* **8**, 1–37.

Branco M, Battisti A and Mendel Z (2016) Foliage feeding invasive insects: defoliators and Gall makers. In TD Paine and F Lieutier. (Eds.) *Insects and diseases of mediterranean forest systems*. Cham, Switzerland: Springer International Publishing, pp. 211–238.

Bush SJ, Dittrich-Schröder G, Neser S, Gevers C, Baffoe KO, Slippers B and Hurley BP (2017) First record of *Quadrastichus Mendeli*, a parasitoid of *Leptocybe invasa*, in South Africa. *Southern Forests*, **80**, 275–277.

Castro L, Austin A and Dowton M (2002) Contrasting rates of mitochondrial molecular evolution in parasitic Diptera and Hymenoptera. *Molecular Biology and Evolution* **19**, 1100–1113.

Collins RA, Boykin LM, Cruickshank RH and Armstrong KF (2012) Barcoding's next top model: an evaluation of nucleotide substitution models for specimen identification. *Methods in Ecology and Evolution* **3**, 457–465.

Darriba D, Taboada GL, Doallo R and Posada D (2012) Jmodeltest 2: more models, new heuristics and parallel computing. *Nature Methods* **9**, 772.

DeSalle R, Egan MG and Siddall M (2005) The unholy trinity: taxonomy, species delimitation and DNA barcoding. *Philosophical Transactions of the Royal Society B: Biological Sciences* **360**, 1905–1916.

Dittrich-Schröder G, Harney M, Neser S, Joffe T, Bush S, Hurley BP, Wingfield MJ and Slippers B (2014) Biology and host preference of *Selitrichodes Neseri*: a potential biological control agent of the *Eucalyptus* Gall wasp, *Leptocybe invasa*. *Biological Control* **78**, 33–41.

Dittrich-Schröder G, Hoareau TB, Hurley BP, Wingfield MJ, Lawson S, Nahrung HF and Slippers B (2018) Population genetic analyses of complex global insect invasions in managed landscapes: a *Leptocybe Invasa* (Hymenoptera) case study. *Biological Invasions* **20**, 2395–2420.

Doğanlar M (2015) Diagnosis of *Megastigmus* Spp. (Hymenoptera: Torymidae) reared from galls of *Leptocybe invasa* FISHER & LASALLE, 2004, (Hymenoptera: Eulophidae) on *Eucalyptus* Spp. (Myrtaceae), with description of a new species from South Africa. *Entomofauna* **36**, 561–580.

Doğanlar M and Hassan E (2010) Review of Australian species of *Megastigmus* (Hymenoptera: Torymidae) associated with *Eucalyptus*, with descriptions of new species. *Australian Journal of Basic and Applied Sciences* **4**, 5059–5150.

Doğanlar M, Huang Z-Y, Guo C-H, Lu W, Yang Z-D, Yang X-H and Zheng X-L (2017) A new species of *Megastigmus* (Hymenoptera: Torymidae: Megastigminae) from China. *Munis Entomology & Zoology* **12**, 368–374.

Evans N and Paulay G (2012) DNA Barcoding methods for invertebrates. In JM Walker. (Ed.) *DNA Barcodes*. New York: Humana Press, pp. 47–77.

FAO (2012) Forest pest species profile – *Leptocybe invasa*. pp. 1–2. http://www.fao.org/forestry/13569-05912e0e2fe9054c3ed4904ae597e3310.pdf

Folmer O, Black M, Hoeh W, Lutz R and Vrijenhoek R (1994) DNA Primers for amplification of mitochondrial cytochrome c oxidase subunit I from diverse metazoan invertebrates. *Molecular Marine Biology and Biotechnology* **3**, 294–299.

Gibson GAP, Read JD and Fairchild R (1998) Chalcid wasps (Chalcidoidea): illustrated glossary of positional and morphological terms. http://www.canacoll.org/Hym/Staff/Gibson/apss/chglintr.htm. (accessed April 2020).

Graham MWRDV (1969) *The Pteromalidae of North-Western Europe (Hymenoptera-Chalcidoidea)*. London: British Museum (Natural History), pp. 9–11.

Grissell EE (1999) *An Annotated Catalog of World Megastigminae (Hymenoptera: Chalcidoidea: Torymidae)*. Gainesville, Florida: American Entomological Institute, p. 93.

Grissell EE (2006) A new species of *Megastigmus* Dalman (Hymenoptera: Torymidae), galling seed capsules of *Eucalyptus Camaldulensis* Dehnhardt (Myrtaceae) in South Africa and Australia. *African Entomology* **14**, 87–94.

Guindon S, Dufayard J-F, Lefort V, Anisimova M, Hordijk W and Gascuel O (2010) New algorithms and methods to estimate maximum-likelihood phylogenies: assessing the performance of PhyML 3.0. *Systematic Biology* **59**, 307–321.

Hajibabaei M, Singer GA, Hebert PD and Hickey DA (2007) DNA Barcoding: how it complements taxonomy, molecular phylogenetics and population genetics. *Trends in Genetics* **23**, 167–172.

Hernández CM, Aquino DA, Cuello EM, Andorno AV and Botto EN (2015) Primera cita de *Megastigmus zebrinus* Grissell de Argentina (Hymenoptera: Torymidae) asociado a agallas de *Leptocybe Invasa* (Hymenoptera: Eulophidae). *Revista de la Sociedad Entomologica Argentina* **74**, 75–77.

Huang Z-Y, Liu J-Y, Zhang Y-J, Guo C-H, Yang Z-D, Lu W and Zheng X-L (2017) Scanning electron microscopy of antennal sensilla of *Megastigmus sichuanensis* Doğanlar et Zheng (Hymenoptera: Torymidae). *Zoologischer Anzeiger* **271**, 25–32.

Huang ZY, Li J, Lu W, Zheng XL and Yang ZD (2018) Parasitoids of the eucalyptus gall wasp *Leptocybe* Spp. a global review. *Environmental Science and Pollution Research* **25**, 29983–29995.

Janšta P, Cruaud A, Delvare G, Genson G, Heraty J, Křížková B and Rasplus J-Y (2018) Torymidae (Hymenoptera, Chalcidoidea) revised: molecular phylogeny, circumscription and reclassification of the family with discussion of its biogeography and evolution of life-history traits. *Cladistics* **34**, 627–651.

Kelly J, La Salle J, Harney M, Dittrich-Schröder G and Hurley BP (2012) *Selitrichodes Neseri* n. sp, a new parasitoid of the eucalyptus gall wasp *Leptocybe Invasa* Fisher & La Salle (Hymenoptera: Eulophidae: Tetrastichinae). *Zootaxa* **3333**, 50–57.

Kim I-K, Mendel Z, Protasov A, Blumberg D and La Salle J (2008) Taxonomy, biology, and efficacy of two Australian parasitoids of the euca-lyptus gall wasp, *Leptocybe Invasa* Fisher & La Salle. *Zootaxa* **1910**, 1–20.

Kumar S, Stecher G, Li M, Knyaz C and Tamura K (2018) MEGA X: molecular evolutionary genetics analysis across computing platforms. *Molecular Biology and Evolution* **35**, 1547–1549.

Lanfear R, Frandsen PB, Wright AM, Senfeld T and Calcott B (2016) Partitionfinder 2: new methods for selecting partitioned models of evolu-tion for molecular and morphological phylogenetic analyses. *Molecular Biology and Evolution* **34**, 772–773.

Le NH, Nahrung HF, Griffiths M and Lawson SA (2018) Invasive *Leptocybe* Spp. and their natural enemies: global movement of an insect fauna on eucalypts. *Biological Control* **125**, 7–14.

Mendel Z, Protasov A, Fisher N and La Salle J (2004) Taxonomy and biology of *Leptocybe Invasa* gen. & sp. n. (Hymenoptera: Eulophidae), an invasive gall inducer on *Eucalyptus. Australian Journal of Entomology* **43**, 101–113.

Mendel Z, Protasov A, La Salle J, Blumberg D, Brand D and Branco M (2017) Classical biological control of two *Eucalyptus* Gall wasps; main out-come and conclusions. *Biological Control* **105**, 66–78.

Milliron HE (1949) Taxonomic and biological investigations in the genus *Megastigmus* with particular reference to the taxonomy of the Nearctic spe-cies (Hymenoptera: Chalcidoidea; Callimomidae). *American Midland Naturalist* **41**, 257–420.

Narendran T and Sureshan P (1988) A contribution to our knowledge of Torymidae of India (Hymenoptera: Chalcidoidea). *Bollettino del Laboratorio di Entomologia Agraria Filippo Silvestri, Portici* **45**, 37–47.

Narendran T, Girish Kumar P and Vastrad A (2010) Two new species of *Megastigmus* Dalman (Hymenoptera: Torymidae) from India, with a revised key to Indian species. *Records of the Zoological Survey of India* **110**, 1–6.

Noyes JS (2020) Universal Chalcidoidea Database. http://www.nhm.ac.uk/chalcidoids.

Nugnes F, Gebiola M, Monti MM, Gualtieri L, Giorgini M, Wang J and Bernardo U (2015) Genetic diversity of the invasive gall wasp *Leptocybe Invasa* (Hymenoptera: Eulophidae) and of its Rickettsia endosymbiont, and associated sex-ratio differences. *PLoS One* **10**, 1–19.

Phạm QT, Dell B and Isobel Burgess T (2009) Susceptibility of 18 eucalypt species to the gall wasp *Leptocybe Invasa* in the nursery and young planta-tions in Vietnam. *ScienceAsia* **35**, 113–117.

Price PW (2005) Adaptive radiation of gall-inducing insects. *Basic and Applied Ecology* **6**, 413–421.

Price PW, Fernandes GW and Waring GL (1987) Adaptive nature of insect galls. *Environmental Entomology* **16**, 15–24.

Protasov A, Doğanlar M, La Salle J and Mendel Z (2008) Occurrence of two local *Megastigmus* species parasitic on the eucalyptus gall wasp *Leptocybe Invasa* in Israel and Turkey. *Phytoparasitica* **36**, 449–459.

Puillandre N, Lambert A, Brouillet S and Achaz G (2012) ABGD, Automatic Barcode Gap Discovery for primary species delimitation. *Molecular Ecology* **21**, 1864–1877.

Ramanagouda S, Vastrad A, Narendran T, Basavanagoud K and Viraktamath S (2011) Current status of eucalyptus gall wasp and its native parasitoids in Karnataka. *Journal of Biological Control* **25**, 193–197.

Ripley B, Venables B, Bates DM, Hornik K, Gebhardt A and Firth D (2018) Support functions and datasets for Venables and Ripley's MASS R package version 7.3-29.

Rokas A, Nylander JA, Ronquist F and Stone GN (2002) A maximum-likelihood analysis of eight phylogenetic markers in gallwasps (Hymenoptera: Cynipidae): implications for insect phylogenetic studies. *Molecular Phylogenetics and Evolution* **22**, 206–219.

Roques A and Skrzypczyńska M (2003) Seed-infesting chalcids of the genus *Megastigmus* Dalman, 1820 (Hymenoptera: Torymidae) native and intro-duced to the West Palearctic region: taxonomy, host specificity and distri-bution. *Journal of Natural History* **37**, 127–238.

Roques, A., R.S. Copeland, L. Soldati, O. Denux and M.-A. Auger-Rozenberg (2016) Megastigmus seed chalcids (Hymenoptera, Torymidae) radiated much more on Angiosperms than previously considered. I-Description of 8 new species from Kenya, with a key to the females of Eastern and Southern Africa. *Zookeys*, 51–124.

RStudio Team (2019) *RStudio: Integrated Development for R*. Boston, MA: RStudio, Inc.

Sangtongpraow B and Charernsom K (2013) Evaluation of parasitism cap-acity of *Megastigmus Thitipornae* Doğănlar & Hassan (Hymenoptera: Torymidae), the local parasitoid of *Eucalyptus* Gall wasp, *Leptocybe Invasa* Fisher & La Salle (Hymenoptera: Eulophidae). *Kasetsart Journal (Natural Science)* **47**, 191–204.

Scheffer SJ and Grissell E (2003) Tracing the geographical origin of *Megastigmus transvaalensis* (Hymenoptera: Torymidae): an African wasp feeding on a South American plant in North America. *Molecular Ecology* **12**, 415–421.

Stamatakis A (2014) RAxML version 8: a tool for phylogenetic analysis and post-analysis of large phylogenies. *Bioinformatics (Oxford, England)* **30**, 1312–1313.

Tavaré S and Miura R (1986) Some mathematical questions in biology: DNA sequence analysis. *Lectures on Mathematics in the Life Sciences* **17**, 57–86.

Viggiani G, Laudonia S and Bernardo U (2002) Aumentano gli insetti dan-nosi agli eucalipti. *Informatore Agrario* **58**, 2.